RSC Advances

PAPER

View Article Online
View Journal | View Issue



Cite this: *RSC Adv.*, 2024, **14**, 7206

# Mechanism of $SO_2/H_2O$ enhanced rare earth tailings catalysts in $NH_3$-SCR at medium and high temperature

Kunling Jiao,[ab] Jiaming Liu,[a] Xiaoyun Jiao,[a] Siying Wang,[a] Jingran Zhang[a] and Wenfei Wu *[ab]

Received 23rd December 2023
Accepted 12th January 2024

DOI: 10.1039/d3ra08782d

rsc.li/rsc-advances

Rare earth tailings (RET) $NH_3$-SCR catalysts were prepared by mechanical and microwave activation of a large amount of rare earth tailings after beneficiation of Bayan Ebo rare earth ore. The effects of $SO_2/H_2O$ on the denitrification performance of the RET catalysts were evaluated by conducting denitrification activity tests, $SO_2/H_2O$ tolerance tests and *in situ* DRIFTs mechanistic analysis. The results showed that the denitrification activity was significantly increased in the presence of $SO_2/H_2O$. And *in situ* DRIFTs analysis showed that in the presence of $SO_2/H_2O$, $SO_2$ could be adsorbed as $SO_3^{2-}$ groups by the hydroxyl groups on the catalyst surface and react with $SO_4^{2-}$ to form $S_2O_7^{2-}$ species. And in the presence of $NH_3$, $S_2O_7^{2-}$ would decompose into unstable $SO_4^{2-}$ species and $SO_3^{2-}$ and continue to react cyclically to form $S_2O_7^{2-}$ species, providing the RET catalyst provides more acid sites, facilitating the SCR reaction.

## 1 Introduction

$NO_x$ is considered to be one of the serious air pollutants and its main source is industrial combustion emissions from fossil fuels in thermal power plants. $NH_3$-SCR technology is an effective method for $NO_x$ removal.[1–3] $V_2O_5$–$WO_3(MoO_3)/TiO_2$ has been used industrially for many years,[4,5] but its applicable denitrification temperature range is narrow. To broaden or reduce the applicable temperature range, researchers have carried out work on the preparation of $NH_3$-SCR catalysts using transition metal elements,[6–13] which mainly focused on Mn-based, Fe-based and rare earth-based catalysts. It was found that Mn-based catalysts have a good De-$NO_X$ activity in the low temperature band but poor $SO_2/H_2O$ tolerance.[6–8] Fe-based catalysts have some activity (lower than Mn-based catalysts) in the medium to high temperature band (150–450 °C) and have better $SO_2$ tolerance.[9–13] Single metal oxide catalysts usually have certain defects, so they are usually loaded with other elements to form composite metal oxides for the preparation of the $NH_3$-SCR catalysts to compensate for each other's defects.

Bayan Ebo has a large amount of rare earth tailings after beneficiation, which contains a rich variety of $NH_3$-SCR active elements (Fe, Ce, Mn),[14] of which rare earth elements are excellent $NH_3$-SCR catalyst active components.[15] In addition, there are congenial relationships such as adjacency, leaching and encapsulation of various active minerals in rare earth tailings, and the interactions that exist between these congenial minerals can also facilitate the SCR reaction process,[16,17] so rare earth tailings are naturally excellent materials that can be used to prepare $NH_3$-SCR catalysts.

$SO_2/H_2O$ poisoning phenomenon seriously affects the activity of SCR catalysts. Due to the increase of $HSO_4^-$ and $SO_4^{2-}$ on the catalyst surface, it often leads to accumulation of ammonium sulfate on the catalyst surface and irreversible sulfation of the active components of the catalyst leading to decreased activity. So improving the $SO_2/H_2O$ tolerance of catalysts is directly related to the practical application of catalysts and is an unavoidable indicator in the evaluation of $NH_3$-SCR catalysts. Composite oxide catalysts doped with rare earth elements exhibit better $SO_2/H_2O$ tolerance and denitrification efficiency compared to Fe-based and Mn-based denitrification catalysts.[18–21] In contrast, rare earth tailings with multiple active components (Fe, Ce, Mn) are natural composite oxides, and rare earth tailings catalysts have better $SO_2/H_2O$ tolerance performance than most composite oxide catalysts.

Therefore, it is necessary to investigate the $SO_2/H_2O$ tolerance characteristics of the Bayan Ebo rare earth tailings catalysts (RET) in the $NH_3$-SCR denitrification process and to investigate the $SO_2/H_2O$ tolerance mechanism in the denitrification process. This paper explores the process and tolerance mechanism of $SO_2/H_2O$ on the denitrification performance of the RET catalysts and expands the research field of $NH_3$-SCR denitrification with rare earth tailings catalysts from Bayan Ebo.

[a]*School of Energy and Environment, Inner Mongolia University of Science and Technology, Baotou, Inner Mongolia Autonomous Region, 014010, China. E-mail: jklgroup1984@163.com*

[b]*Key Laboratory of Efficient and Clean Combustion, Inner Mongolia, China*

Table 1 Rare earth tailings catalyst (RET) XRF results

| Element | Fe | Ca | Si | Mg | Ce | Al | Mn | Other |
|---|---|---|---|---|---|---|---|---|
| Percentage (%) | 17.394 | 17.798 | 8.804 | 3.104 | 1.783 | 1.485 | 0.926 | 48.706 |

# 2 Materials and methods

## 2.1 Catalysts preparation

The rare earth tailings catalyst was prepared by ball mills. And the rare earth tailings come from Bayan Ebo (Baotou, China). The beneficiated rare earth tailings material was fixed in a canister on a planetary ball mill and ball milled at 300 rpm for 2 h. The obtained material was passed through a 200 mesh sieve and microwave roasted at 1100 w, 250 °C for 20 min to obtain the catalyst powder. The elemental content of the catalyst was quantified by XRF. As shown in Table 1, the results of the XRF analysis, in which Fe, Ca, Si, Mg, Ce and Al were the major elements with a total content of 50.4%, and the remaining 49.6% are Mn and other trace elements, and the content of each trace element is <1%. The Bayan Ebo rare earth tailings catalyst is indicated as RET.

## 2.2 Catalytic performance experiment

The $NH_3$-SCR performance experiments with the RET catalysts were carried out in a SCR denitrification evaluation unit, as shown in Fig. 1. The denitrification evaluation unit is consisted of gas distribution system (1–4), reaction system (5–8) and analysis system (9–11), and is equipped with a tail gas treatment unit (12). The sample is fixed in a 9 mm inner diameter quartz fixed bed reaction tube. The reaction gas mixture consists of NO (500 ppm), $NH_3$ (500 ppm), $H_2O$ (6 vol% when in use), $SO_2$ (500 ppm when in use), $O_2$ (6 vol%) and $N_2$ are controlled by the gas distribution system at a flow rate (100 mL $min^{-1}$), and the GHSV are set to 30 000 $h^{-1}$. The gas mixture were measured by on-line multi-component flue gas analyzer (HP-OMGA, China), the measurement accuracy is ≤± 2% FS, and the $NO_X$ conversion is obtained from the formula (1):

$$NO_x\ \text{conversion}(\%) = \frac{[NO_x]_{in} - [NO_x]_{out}}{[NO_x]_{in}} \times 100\% (x = 1, 2) \quad (1)$$

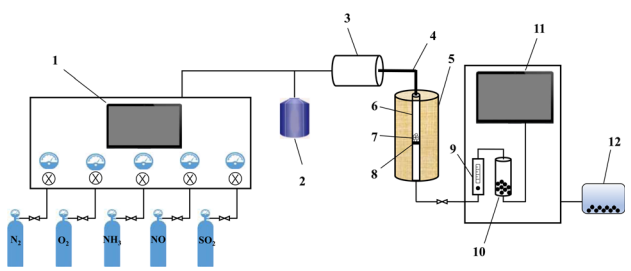


Fig. 1 Schematic diagram of the $NH_3$-SCR evaluation unit ((1) gas flow control system; (2) heating water tank; (3) gas distribution tank; (4) heating pipes; (5) heating furnace; (6) quartz tubes; (7) RET catalyst; (8) quartz wool; (9) rotameter; (10) condensation drying device; (11) flue gas online detection device; (12) tail gas treatment device).

## 2.3 Catalysts characterization

The RET catalysts were characterization by the X-ray diffraction (XRD), temperature programmed reduction by $H_2$ and $NH_3$ ($H_2$-TPR and $NH_3$-TPD), and *in situ* Diffuse Reflectance Infrared Fourier Transform Spectroscopy (DRIFTS).

# 3 Results and discussion

The RET catalysts after denitrification under different operating conditions were characterised as sample 0, 1, 2 and 3. The total flow rate for all operating condition cases is 100 mL $min^{-1}$, as shown in Table 2.

## 3.1 Structural changes of catalysts

As shown in Fig. 2, the diffraction peaks of fluorite ($CaF_2$), quartz ($SiO_2$), aluminium trioxide ($Al_2O_3$), iron dolomite {$Ca(MgFe)[(CO_3)_2]$}, hematite ($Fe_2O_3$) and cerium fluoride ($CeCO_3F$) were mainly detected on the surface of sample 0, where the $Ca(MgFe)[(CO_3)_2]$, $Fe_2O_3$ and $CeCO_3F$ diffraction peaks are overlap, it is due to the natural action of these reactive minerals to form a solid solution structure.[18,19] In comparison to sample 0, no significant crystalline phase changes were observed for sample 1 when the catalyst was reacted under $H_2O$ conditions for 24 hours. However, when the catalyst was reacted

Table 2 Working conditions for the preparation of the four RET catalysts

| Catalysts | $NH_3$/ppm | NO/ppm | $O_2$/% | $H_2O$/% | $SO_2$/ppm |
|---|---|---|---|---|---|
| Sample 0 | 500 | 500 | 6 | — | — |
| Sample 1 | 500 | 500 | 6 | 6 | — |
| Sample 2 | 500 | 500 | 6 | — | 500 |
| Sample 3 | 500 | 500 | 6 | 6 | 500 |

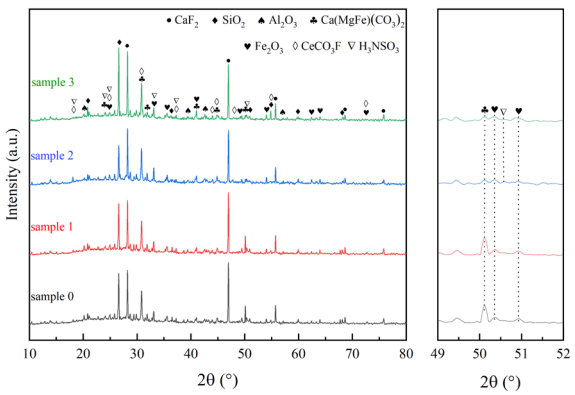


Fig. 2 Rare earth tailings catalyst (RET) XRD results.

under $SO_2$ or $SO_2$ and $H_2O$ conditions for 24 hours, a decrease in the intensity of the Ca(MgFe)[$(CO_3)_2$] and $Fe_2O_3$ diffraction peak intensities was found for samples 2 and 3, but no characteristic metal sulphate peaks were detected, indicating that the $SO_2$ sulphide phase was present in an amorphous form and could not be observed by XRD. However, in the presence of $SO_2$ or $SO_2$/$H_2O$, new diffraction peaks were observed for samples 2, 3 at 18.43°, 24.17°, 24.84°, 33.14°, 37.02° and 50.68°, which can be attributed to sulphonate ($NH_3SO_3$) (PDF#08-0483). And these diffraction peaks overlap with or are similar to the active mineral diffraction peaks of Ca(MgFe)[$(CO_3)_2$], $Fe_2O_3$ and $CeCO_3F$. It can be inferred that the newly formed crystalline phase $NH_3SO_3$ is produced because the acid groups formed on the catalyst surface after $SO_2$/$H_2O$ is involved in the denitrification process and during the drop to low temperature interact with the $NH_3$ adsorbed species and a reduction reaction occurs to reduce the active metal centres in the active minerals to their original state.[22–24]

### 3.2 Catalyst performance change

To examine the effect of $SO_2$/$H_2O$ on the $NH_3$ adsorption of the RET catalyst as shown in Fig. 3. The peak temperatures of the desorption peaks of sample 0 were 147 °C (weak acid centers), 356 °C (medium centers) and 480 °C (strong centers).[25] The $NH_3$ adsorption capacity of samples 1, 2 and 3 was significantly higher than sample 0, while the $NH_3$ adsorption capacity of samples 2 and 3 was slightly higher than sample 1. Sample 0 showed a desorption peak at 147 °C corresponding to the weak acid site, a desorption peak at 356 °C corresponding to at the medium to strong acidic site, and a desorption peak at 480 °C corresponding to the strong acidic site. At 480 °C corresponds to the desorption peak from the strongly acidic site. Samples 1, 2 and 3 also showed three peaks in the low and medium-high temperature sections, each acidic site being shifted back and enhanced compared to sample 0, indicating that the presence of a suitable amount of $SO_2$/$H_2O$ can strengthen the acidic sites on the RET catalyst. The peak at 150 °C for sample 3, which was influenced by the combined presence of $SO_2$/$H_2O$, was attributed to the weakly acidic sites, with a significantly greater ability to adsorb $NH_3$ on the weakly acidic sites relative to the RET

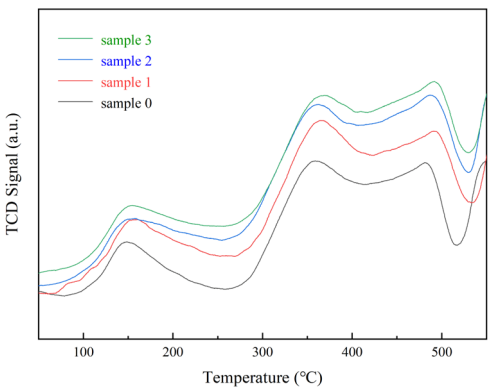


Fig. 3 Rare earth tailings catalyst (RET) $NH_3$-TPD results.

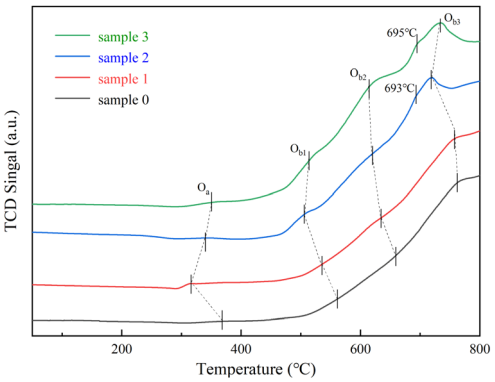


Fig. 4 Rare earth tailings catalyst (RET) $H_2$-TPR results.

catalysts influenced by the presence of $SO_2$ or $H_2O$ alone with larger desorption peaks at 365 °C and 489 °C attributed to the moderately strong and strong acidic sites. Significantly larger peak areas in the mid to high temperature fractions compared to samples 1 and 2, which were affected by $SO_2$/$H_2O$ alone. It means that co-modification of $SO_2$ and $H_2O$ can also substantially enhance the ability of medium to strong acidic sites to adsorb $NH_3$. Overall, the RET catalyst with the influence of $SO_2$/$H_2O$ both increased the acidic sites and improved $NH_3$ adsorption capacity. Combined with XRD analysis, it was found that the increase in acidic sites after the catalyst was affected by $SO_2$/$H_2O$ can be attributed to the formation of $NH_3SO_3$, which is readily decomposed by heat, thus providing more acidic sites.

$H_2$-TPR tests were using to investigate the effect of the $SO_2$/$H_2O$ on the redox ability of the RET catalyst. In Fig. 4, the $O_a$ peak located below 400 °C is the reduction peak of oxygen species adsorbed on the catalyst surface. The $O_{b1}$ peak located between 400 and 600 °C is the peak of $H_2$ consumption ($Fe_2O_3$ to $Fe_3O_4$ and the reduction of the $CeO_2$).[26,27] The $O_{b2}$ peak between 600 and 700 °C is the peak of $H_2$ consumption ($Fe_3O_4$ to FeO).[26] The $O_{b3}$ peak above 700 °C is the peak of $H_2$ consumption (FeO to Fe).[26] The reduction peaks of the RET catalysts with $SO_2$ or $SO_2$/$H_2O$ are shifted towards a lower temperature region and the peak area is slightly increased compared to the RET catalysts without the influence of $SO_2$ or $H_2O$. This means that $SO_2$ and $H_2O$ can influence the RET catalysts to induce a beneficial change in redox capacity towards a more beneficial catalytic reduction reaction occurring, with new shoulder peaks are due to the reduction of the $CeO_2$ at 693 °C and 695 °C,[27] and the introduction of $SO_2$/$H_2O$ leads to a more pronounced shoulder peak shape at 695 °C. Which combined with XRD analysis, is presumed to be due to the influence of $SO_2$, which induces the reduction of RET catalysts with the natural co-occurrence of active minerals associated properties of the RET catalyst resulted from the joint participation of multiple substances in the redox reaction.[28] From the $H_2$-TPR results, electron transfer paths can be derived ($Fe^{3+} \leftrightarrow Fe^{2+}$ and $Ce^{4+} \leftrightarrow Ce^{3+}$).

The surface of the rare earth tailings catalyst (Fig. 5a) showed an uneven and pitted morphology, and the surface of the rare earth tailings catalyst (Fig. 5b) did not change much after the

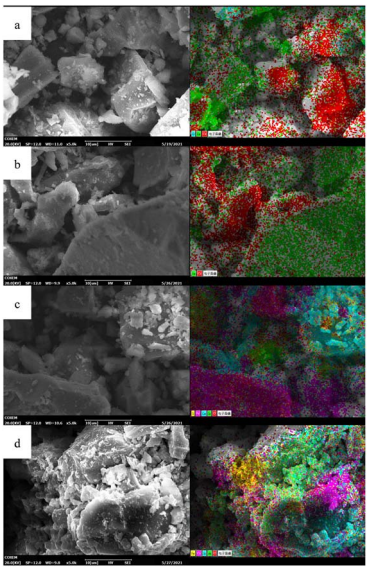


Fig. 5 SEM and EDS surface sweeps before and after the effect of $SO_2$/$H_2O$ on RET catalysts ((a) fresh RET catalyst; (b) after $H_2O$; (c) after $SO_2$; (d) after $SO_2$/$H_2O$).

$H_2O$ tolerance test. After being affected by $SO_2$ alone and $SO_2$/$H_2O$ tolerance, the catalysts (Fig. 5c and d) showed some mobility, which was in the form of stacked lamellar fragmentation with a few fine particles attached to the surface, after being affected by $SO_2$/$H_2O$ tolerance, there was a large volume of lamellar particles stacked on the surface of the catalysts, and after the catalysts were affected by the simultaneous presence of $SO_2$ and $H_2O$, the lamellar particles were attached to the surface of the catalysts.

### 3.3 *In situ* DRIFTs analysis

**3.3.1 Effect of $H_2O$ on the adsorption of $SO_2$ on the catalyst surface.** The adsorption of $SO_2$ in the presence of $H_2O$ at 350 °C was investigated by *in situ* DRIFTS, as shown in Fig. 6.

As shown in Fig. 6, the RET catalyst was exposed to $SO_2$/$O_2$ for 60 min and treated in a pure $N_2$ gas stream (100 mL $min^{-1}$) at 350 °C for a further 30 min. 5 min after the addition of $H_2O$, an absorption peak of molecular water (1647 $cm^{-1}$) appeared, with little change in peak intensity with increasing time, meaning that the $H_2O$ tolerance of the RET catalyst was good. The absorption peak of sulfite (1434 $cm^{-1}$) disappeared with increasing time and the absorption peak of pyrosulfate (1396 $cm^{-1}$) gradually became stronger. The absorption peaks of bridged tri-dentate sulphate (1326 $cm^{-1}$), double-dentate sulphate (1076 $cm^{-1}$), bridged double-dentate sulphate (1197 $cm^{-1}$) and single-dentate sulphate (1261 $cm^{-1}$) showed little change.[31,32,35,36] The crystalline water variable angle vibrational peak shifted from 1535 to 1581 $cm^{-1}$, it is due to the chemisorption of gaseous $SO_2$ onto the catalyst surface *via* hydroxyl groups.[37] The increase in persulphate is due to the presence of $H_2O$, which causes the formation of hydroxyl groups on the RET catalyst surface, and adsorb more $SO_2$ to form $SO_3^{2-}$, which in turn reacts with the catalyst surface sulphate species to form $S_2O_7^{2-}$, so $H_2O$ promotes the formation of $S_2O_7^{2-}$ species on the RET catalyst surface.

**3.3.2 Effect of $SO_2$/$H_2O$ on surface acidity.** Fig. 7 shows that $NH_3$ was first adsorbed without $SO_2$ for 60 min at 350 °C and then treated in a pure $N_2$ gas stream (100 mL $min^{-1}$) for a further 30 min.

Fig. 7 shows the absorption peaks of $NH_4^+$ adsorption at the Brønsted acid site (1392, 1427, 1461, 1500 $cm^{-1}$), $NH_3$ adsorption at the Lewis acid site (1025, 1157, 1228, 1620 $cm^{-1}$) and it causes $NH_3$ form –$NH_2$ (1332 $cm^{-1}$).[29,30] After continuing the ammonia stream and 5 min of $SO_2$, $H_2O$ and $O_2$, the absorption peaks of $NH_4^+$ adsorption (1392, 1461 $cm^{-1}$) and $NH_3$ adsorption at the Lewis acid site (1157, 1228, 1620 $cm^{-1}$) disappeared. The intermediate product –$NH_2$ (1529 $cm^{-1}$)[29,30] and $NH_3$ adsorption (1600 $cm^{-1}$)[29,30] with increasing peak intensity with time, meaning that the presence of $SO_2$/$H_2O$ promoted $NH_3$ adsorption. Bidentate sulfate (1068 $cm^{-1}$), bridged bidentate sulfate (1191 $cm^{-1}$), and monodentate sulfate (1265 $cm^{-1}$) absorption peaks were also present after 40 min.[31,35,36] The intensity of the bidentate and bridged bidentate sulfate absorption peaks frequently changes but no pyrosulfate species were found at 1391 $cm^{-1}$. In combination with XRD analysis, was attributed to the formation of $NH_3SO_3$ from $NH_3$ adsorbed species bound to the catalyst surface. After 40 min of addition of $SO_2$, $H_2O$ and $O_2$, the intermediate product –$NH_2$ (1300,

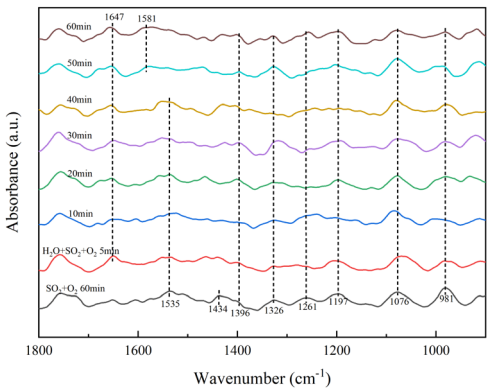


Fig. 6 Effect of $H_2O$ on the adsorption of $SO_2$ by the RET catalyst.

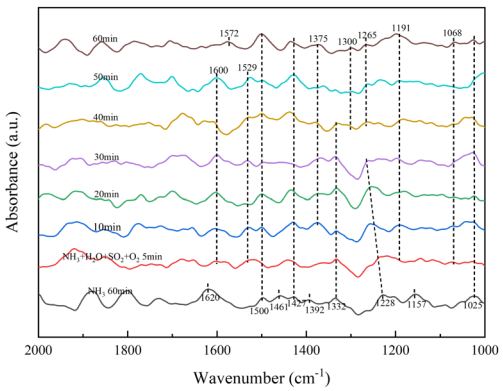


Fig. 7 Effect of $SO_2$/$H_2O$ on catalyst $NH_3$ adsorption.

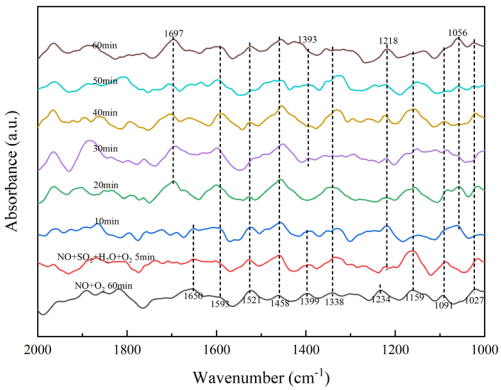


Fig. 8 Effect of $SO_2/H_2O$ on NO adsorption by RET catalysts.

1572 $cm^{-1}$) appeared, resulting from the creation of a new Lewis acid site, which is consistent with $NH_3$-TPD results. $SO_2/H_2O$ caused the formation of an unstable sulphate species, which adsorbed on the active metal sites are strongly acidic, so this unstable sulphate species provides more acidic sites for the $NH_3$-SCR process and is less likely to form ammonium sulphate species with $NH_3$. The combination of $NH_3$ with catalyst surface species to form $NH_3SO_3$ resulted in the disappearance of persulphate species from the RET catalyst surface, indicating that the presence of $NH_3$ promoted the decomposition of $S_2O_7^{2-}$.

**3.3.3 Effect of $SO_2$ on the adsorbed NO species.** As in step with Fig. 8, the *in situ* DRIFTS spectra showed the effect of $SO_2/H_2O$ on NO adsorption on the RET catalyst at 350 °C.

In Fig. 8, the addition of NO and $O_2$ gas streams followed by a pure $N_2$ gas stream shows monodentate nitrite (1027, 1091, 1159 $cm^{-1}$), bridged nitrite (1234 $cm^{-1}$), intermediate product-$NO_2$ (1338, 1399, 1458 $cm^{-1}$), intermediate product-$NO_3$ (1521 $cm^{-1}$) and adsorbed $NO_2$ (1593, 1650 $cm^{-1}$).[33,34] After simultaneous introduction of NO, $O_2$, $H_2O$ and $SO_2$ for 5 min, the absorption peak of bridged nitrite shifted from 1234 to 1218 $cm^{-1}$ with little change in peak intensity with increasing time, with bridged nitrite still occupying the active site. After 10 min of addition of $H_2O$ and $SO_2$, the absorption peaks of –$NO_2$ (1399 $cm^{-1}$) and adsorbed $NO_2$ (1650 $cm^{-1}$) disappeared and absorption peaks of bidentate sulfate (1056 $cm^{-1}$), pyrosulfate (1393 $cm^{-1}$) and $NO_2$ (1697 $cm^{-1}$) generated by the reaction of adsorbed NO on the surface appeared.[33,34,38] In the presence of $SO_2/H_2O$, the absorption peak of $S_2O_7^{2-}$ species gradually increased with time and the –$NO_2$ disappeared, due to the competition between $SO_2$ and NO adsorption on this active site to produce $S_2O_7^{2-}$ species. It occupies part of the NO adsorption site, and the increase in surface active oxygen species due to $SO_2$ acidification of the RET catalyst, converting more NO to $NO_2$ and hence the absorption peak of $NO_2$.

**3.3.4 Transient reactions of $NH_3$ and NO on the catalyst surface.** As shown in Fig. 9a, the *in situ* DRIFTs spectra of the reaction of NO with pre-adsorbed $NH_3$ species on the RET catalyst surface under the influence of $SO_2/H_2O$ and Fig. 9b shows the *in situ* DRIFTs spectra of the reaction of $NH_3$ with pre-adsorbed NO species on the RET catalyst surface under the influence of $SO_2/H_2O$.

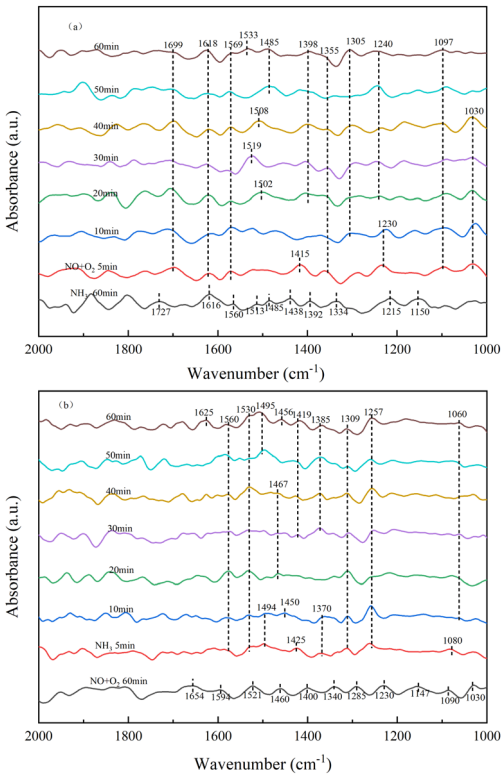


Fig. 9 RET Catalytic transient reaction in the presence of $SO_2/H_2O$ ((a) $NH_3$/NO; (b) NO/$NH_3$).

As shown in Fig. 9a, the RET catalysts were firstly exposed to $NH_3$ gas flow for 60 min in the addition of $SO_2/H_2O$, and then purged with $N_2$ at 350 °C for 20 min.

Fig. 9a shows the absorption peaks of $NH_4^+$ adsorption (1392, 1438, 1485, 1513, 1727 $cm^{-1}$), $NH_3$ adsorption (1150, 1215, 1616 $cm^{-1}$) and –$NH_2$ (1334, 1560 $cm^{-1}$).[29,30] After 5 min of the addition of NO and $O_2$, the $NH_3$ adsorbed species disappeared and peaks appeared for monodentate nitrite (1030, 1097 $cm^{-1}$), bridged nitrite (1230 $cm^{-1}$), intermediate product –$NO_2$ (1355, 1415, 1618 $cm^{-1}$), bidentate nitrate (1569 $cm^{-1}$) and $NO_2$ (1699 $cm^{-1}$).[33,34] The peak of –$NO_2$ (1415 $cm^{-1}$) disappeared rapidly with increasing time. The peak pattern of bridged nitrite shifted from 1230 to 1240 $cm^{-1}$ with little change in peak intensity. Monodentate nitrite (1097 $cm^{-1}$) and bidentate nitrate (1569 $cm^{-1}$) showed little change. Absorption peaks for intermediate product-$NO_2$ (1305, 1398 $cm^{-1}$) and intermediate product-$NO_3$ (1502 $cm^{-1}$) appeared after 20 min of the addition of NO/$O_2$. Absorption peaks of –$NO_3$ at 1519, 1508, 1485 and 1533 $cm^{-1}$ appeared, with significant changes in peak pattern with increasing time. The absorption peaks of –$NO_2$ did not change much after 20 min of NO/$O_2$ addition, and the peak intensity increased. This is due to the fact that when NO/$O_2$ were first added, the $NH_3$ adsorbed species mainly combined with –$NO_2$ to form the intermediate product, and after 20 min as NO was oxidized to more $NO_2$, the –$NO_3$ group was generated to participate in the reaction. The results show that –$NO_2$ is easier to combine with $NH_4^+$ than –$NO_3$ to form the intermediate product $NH_4NO_2$. And when $NH_3$ is present, the NO species

mainly form the $-NO_2$ group directly to participate in the reaction, without oxidation between the catalyst and $NO_2$ to form the $-NO_3$ group, shortening the reaction process in favor of the $NH_3$-SCR reaction.

In Fig. 9b, the samples were first exposed to NO and $O_2$ for 60 min in the presence of $SO_2/H_2O$, and then treated in a pure $N_2$ gas stream (100 mL $min^{-1}$) at 350 °C for a further 30 min. The appearance of monodentate nitrite (1030, 1090, 1147 $cm^{-1}$) was observed in Fig. 9b, with bridging nitrite (1230 $cm^{-1}$), $-NO_2$ (1285, 1340, 1400, 1460 $cm^{-1}$), $-NO_3$ (1521 $cm^{-1}$) and adsorbed $NO_2$ (1594, 1654 $cm^{-1}$) absorption peaks.[33,34] After 5 min of the addition of $NH_3$, the peaks of the nitrate-like adsorbed species, adsorbed state $NO_2$, intermediate products $-NO_2$ and $-NO_3$ disappeared, along with the peaks of adsorbed $NH_4^+$ (1370, 1425, 1494 $cm^{-1}$), adsorbed $NH_3$ (1080, 1257 $cm^{-1}$) and $-NH_2$ (1309, 1530, 1560 $cm^{-1}$),[29,30] where the absorption peak of $-NH_2$ increased in intensity with time. The peak of adsorbed $NH_3$ was less variable, and the peak of adsorbed $NH_4^+$ disappeared quickly. Absorption peaks for $NH_4^+$ (1385, 1419, 1456, 1467, 1495 $cm^{-1}$) and $-NH_2$ (1625 $cm^{-1}$) adsorbed at the Brønsted acid site appeared after 20 min of the addition of $NH_3$.[29,30] When $NH_3$ was present, the $-NO_2$ and $-NO_3$ groups as well as the adsorbed $NO_2$ disappeared from the catalyst surface and $NH_4^+$ and $-NH_2$ groups were generated at subsequent time periods of the reaction, indicating that intermediate products $NH_4NO_3$, $NH_4NO_2$ and $NH_2NO_2$ were generated on the RET catalyst surface to remove NO adsorption products, suggesting that both the E–R mechanism and the L–H mechanism, which acted together to remove $NO_x$ through both pathways.

## 4 Denitrification mechanism of $SO_2/H_2O$ enhanced rare earth tailings catalyst

Combining the results of *in situ* DRIFTs analysis and $SO_2$ characterization,[22,23,38,39] We can surmise the following reaction mechanism (Fig. 10) as well as reaction equations (eqn (2)–(16)) can be derived for the effect of $SO_2/H_2O$ on the RET catalysts. As shown in Fig. 10, combined with the analysis of the $H_2$-TPR results, it is found that the conversion between $Fe^{3+} \leftrightarrow Fe^{2+}$ and $Ce^{4+} \leftrightarrow Ce^{3+}$ on the RET catalyst surface provides the active sites for SCR catalytic denitrification, and the conversion between $Ce^{3+}$ and $Ce^{4+}$ mainly acts as oxygen storage and release (eqn (2)–(5)). When $SO_2/H_2O$ is added, $SO_2$ is adsorbed by the hydroxyl groups formed by $H_2O$ and reacts with $O_2$ to form $SO_3^{2-}$ groups, while combining with $SO_4^{2-}$ groups to form $S_2O_7^{2-}$ (eqn (7)–(9)). When $NH_3$ and NO are present, they are converted to $NH_4^+$ and $NO_2^-$ respectively, which are then reduced to $N_2$ and $H_2O$ (eqn (10)–(15)). The adsorption of $H_2O$ by the catalyst surface increases the –OH sites on the catalyst surface, leading to easier adsorption and conversion of $SO_2$ to form $SO_3^{2-}$, while the $S_2O_7^{2-}$ group is converted to $NH_3SO_3$ and the unstable $SO_4^{2-}$ group by the reduction of $NH_3$ (eqn (16)), allowing the catalyst reactive sites on the surface are restored, inhibiting the continued sulphation of the catalyst surface. $NH_3$ also adsorbs to the Brønsted and Lewis acidic sites on the RET catalyst surface as $-NH_2$ and $NH_4^+$, and perform $NH_3$-SCR reaction.

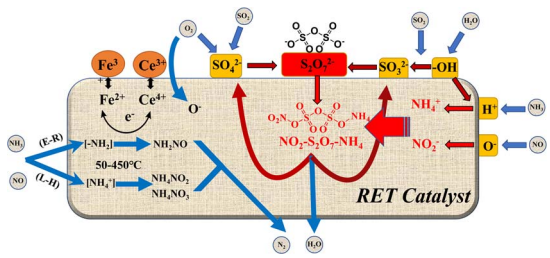


Fig. 10 Mechanism of $SO_2/H_2O$ influence on the surface of rare earth tailings (RET) catalysts (△ represents the active metal sites on the RET catalyst surface; blue arrows represent the gas absorption and release process; black arrows represent the internal electron transfer process of the catalyst; red arrows represent the reaction cycle process of the $S_2O_7^{2-}$ group).

$$Fe^{3+} \leftrightarrow Fe^{2+} + \triangle \quad (2)$$

$$O_{2(g)} + 2\triangle \rightarrow 2O - \triangle \quad (3)$$

$$Ce^{3+} + O_{2(g)} \leftrightarrow Ce^{4+} + 2O^- \quad (4)$$

$$O^- + \triangle \rightarrow O - \triangle \quad (5)$$

$$H_2O_{(g)} + \triangle \rightarrow \triangle - OH + H^+ \quad (6)$$

$$\triangle - OH + SO_{2(g)} \rightarrow \triangle - SO_3^{2-} + H_2O \quad (7)$$

$$2SO_{2(g)} + 3/2O_{2(g)} + H_2O \rightarrow 2SO_4^{2-} + 2H^+ \quad (8)$$

$$SO_4^{2-} + \triangle - SO_3^{2-} \rightarrow \triangle - S_2O_7^{2-} \quad (9)$$

$$\triangle - S_2O_7^{2-} + H^+ \rightarrow \triangle - S_2O_7^{2-}H^+ \quad (10)$$

$$\triangle - S_2O_7^{2-}H^+ + NH_{3(g)} \rightarrow \triangle - S_2O_7^{2-}NH_4^+ \quad (11)$$

$$\triangle - S_2O_7^{2-}NH_4^+ + NO_{(g)} + 1/2O_{2(g)} \rightarrow \triangle - NO_2^- S_2O_7^{2-}NH_4^+ \quad (12)$$

$$\triangle - NO_2^- S_2O_7^{2-}NH_4^+ \rightarrow \triangle - S_2O_7^{2-} + N_{2(g)} + 2H_2O \quad (13)$$

$$\triangle - S_2O_7^{2-} + NH_{3(g)} \rightarrow \triangle - H_2NS_2O_7^{2-}H^+ \quad (14)$$

$$\triangle - H_2NS_2O_7^{2-}H^+ + NO_{(g)} \rightarrow \triangle S_2O_7^{2-}H^+ + N_{2(g)} + H_2O \quad (15)$$

$$\triangle - S_2O_7^{2-}H^+ + NH_{3(g)} + H^+ \rightarrow NH_3SO_3 + SO_4^{2-} + \triangle \quad (16)$$

where △ represents the surface oxygen vacancy in the active metal center. The symbol (g) represents NO, $NH_3$, $SO_2$, $NO_2$, $N_2$, and $O_2$ in the gaseous state. The symbol (a) represents the adsorbed state of $NH_3$, $NH_4^+$ and $SO_3$ on the catalyst surface.

## 5 Catalyst performance

### 5.1 Effect of $H_2O$ and $SO_2$ on catalytic $NO_X$ reduction

The effect of $SO_2/H_2O$ on the catalytic denitrification activity of the RET catalyst was studied in the temperature range of 50–

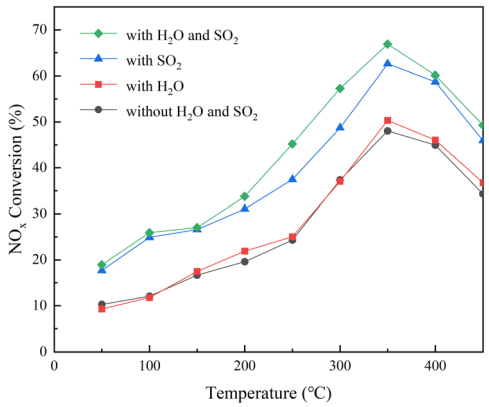


Fig. 11 RET catalyst $NO_X$ removal rate.

450 °C with $\varphi$NO, $\varphi NH_3$ and $\varphi SO_2$ of 500 × $10^{-6}$, $\varphi O_2$ of 6 × $10^{-2}$ and $\varphi H_2O$ of 6 × $10^{-2}$. After the SCR reactor outlet $\varphi$NO was stabilized for 10 min, the $NH_3$ was started to be introduced and the denitrification rate for each temperature section was calculated as the average of the $NO_X$ outlet concentration values within 180 min of stabilization were calculated and the results, as shown in Fig. 11.

Fig. 11 shows that the $NO_X$ conversion of the RET catalyst in the absence of $SO_2/H_2O$ and $SO_2$ is much lower than that in the presence of $SO_2$ and $H_2O$, and $H_2O$ has almost no effect on the $NO_X$ conversion of the RET catalyst. At relatively low temperatures (50 to 200 °C), the enhancement of catalytic activity in the presence of $SO_2$ and $H_2O$ was similar, about 10 ± 1%. However, when the reaction temperature is in the medium to high temperature range (250–450 °C), the activity enhancement under $SO_2/H_2O$ can reach 16 ± 1%, and the activity enhancement of the RET catalyst in $SO_2$ only condition is only 10 ± 1%. Furthermore, at 350 °C, $SO_2/H_2O$ in the gas supply leads to a significant increase in SCR activity of about 18 ± 1%, with a $NO_X$ conversion of 66 ± 1% for the RET catalyst. This enhancement is due to $SO_2$ gas phase acidification of the active metal oxides under $SO_2$.[37] It suggests that the appropriate conditions of $SO_2/H_2O$ presence are favorable to improve the catalytic activity of the RET catalysts.

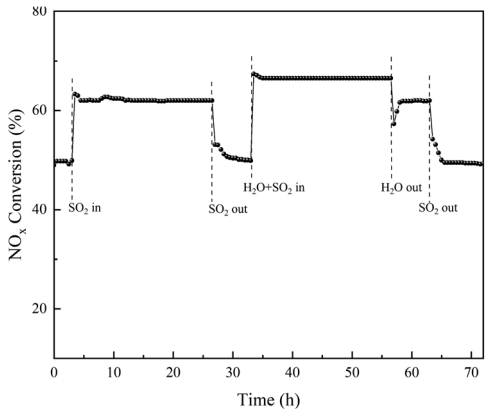


Fig. 12 Stability of RET catalyst $NO_X$ removal rates under the influence of $SO_2/H_2O$.

With the same steps, the stability of the effect of $SO_2/H_2O$ on the $NO_X$ conversion in the temperature range of 350 °C of the RET catalyst over time is shown in Fig. 12 (the data points in the figure are the average values of $NO_X$ conversion over 30 min).

Fig. 12 showed stable catalytic activity at 350 °C during the 72 h test. When $SO_2$ was added to the gas stream, the $NO_X$ conversion increased from a stable 49 ± 1% in the first 3 h to obtain a stable $NO_X$ conversion of 62 ± 1% in 24 h, indicating that $SO_2$ has a significant effect on the catalyst activity. The addition of $SO_2/H_2O$ increases the catalytic activity from 49 ± 1% to 66 ± 1%. However, when $H_2O$ is removed from the gas, the activity can be restored, implying that the enhancement effect of $H_2O$ in promoting $SO_2$ influence on the activity is reversible. The $NO_X$ conversion of the RET catalyst can be recovered when there is no $SO_2$ or $H_2O$ in the reaction gas mixture, which proves that the RET catalyst has a good effect on $SO_2/H_2O$, and the SCR activity of the RET catalyst can be obtained at 350 °C with a 17 ± 1% enhancement under the conditions of both $SO_2$ and $H_2O$.

## 6 Conclusion

In summary, this paper prepared rare earth tailings (RET) catalysts from Bayan Ebo rare earth tailings by ball milling and microwave roasting, and analyzed the $SO_2/H_2O$ tolerance mechanism of the RET catalysts by activity testing, characterization and *in situ* DRIFTs experiments. And revealed the mechanism of $SO_2/H_2O$ to enhance the denitrification performance of catalysts by promoting the cyclic reaction of $S_2O_7^{2-}$ groups on the RET catalysts surface. Although RET catalysts are less active, they can be used as a catalyst active carrier through their excellent $SO_2$ tolerance properties.

(1) The effect of $SO_2/H_2O$ on the RET catalyst was facilitated, and the $NO_X$ conversion of the RET catalyst increased from 48% to 66 ± 1% at 350 °C under $SO_2/H_2O$, which was higher than that of $SO_2$ or $H_2O$ alone.

(2) Rare earth tailings catalyst $NH_3$-SCR denitrification followed the combined L–H and E–R mechanism. The $Fe^{n+}$–$Ce^{n+}$ coactivation of the RET catalyst provides Brønsted and Lewis acid sites.

(3) The effect of $SO_2$ on the RET catalyst is mainly the formation of $SO_4^{2-}$ and $SO_3^{2-}$ species, while $H_2O$ promotes the formation of hydroxyl groups and facilitates $SO_2$ adsorption to form $SO_3^{2-}$, which promotes the reaction of $SO_3^{2-}$ with $SO_4^{2-}$ to form $S_2O_7^{2-}$ groups, which provide acid sites for the RET catalyst and improve the adsorption of $NH_3$. At the same time, the $S_2O_7^{2-}$ group decomposes into $SO_3^{2-}$ and unstable $SO_4^{2-}$ groups, thus continuing the cyclic reaction to form $S_2O_7^{2--}$ groups, thereby increasing the denitrification activity of the RET catalyst activity and inhibit the continued sulphation of the catalyst surface.

## Conflicts of interest

There are no conflicts to declare.

## Acknowledgements

The research was financially supported by the Natural Science Foundation of Inner Mongolia (Grant No. 2019ZD13).

## References

1 K. Skalska, J. S. Miller and S. Ledakowicz, Trends in NOx abatement: A review, *Sci. Total Environ.*, 2010, **408**(19), 3976–3989.

2 G. L. Manney, L. Froidevaux, J. W. Waters, R. W. Zurek, W. G. Read, L. S. Elson, J. B. Kumer, J. L. Mergenthaler, A. E. Roche, A. O'Neill, R. S. Harwood, I. Mackenzie and R. Swinbank, Chemical depletion of ozone in the Arctic lower stratosphere during winter 1992-93, *Nature*, 1994, **370**(6489), 429–434.

3 D. Maric and J. P. Burrows, Formation of $N_2O$ in the photolysis/photoexcitation of NO, $NO_2$ and air, *J. Photochem. Photobiol., A*, 1992, **66**(3), 291–312.

4 H. Bosch and F. Janssen, Catalytic reduction of nitrogen oxides-A review on the fundamental and technology, *Catal. Today*, 1988, **2**(4), 369–532.

5 G. Busca, L. Lietti, G. Ramis and F. Berti, Chemical and mechanistic aspects of the selective catalytic reduction of NOx by ammonia over oxide catalysts: A review, *Appl. Catal., B*, 1998, **18**(1–2), 1–36.

6 F. Kapteijn, L. Singoredjo and A. Andreini, Activity and selectivity of pure manganese oxides in the selective catalytic reduction of nitric oxide with ammonia, *Appl. Catal., B*, 1994, **3**(1), 173–189.

7 T. S. Park, S. K. Jeong, S. H. Hong and S. C. Hong, Selective catalytic reduction of nitrogen oxides with $NH_3$ over natural manganese ore at low temperature, *Ind. Eng. Chem. Res.*, 2001, **40**(21), 4491–4495.

8 L. Singoredjo, R. Korver and F. Kapteijin andJ.Moulijn, Alumina supported manganese oxides for the low-temperature selective catalytic reduction of nitric oxide with ammonia, *Appl. Catal., B*, 1992, **1**(4), 297–316.

9 C. Liu, S. Yang, L. Ma, Y. Peng, A. Hamidreza, H. Chang and J. Li, Comparison on the Performance of alpha-$Fe_2O_3$ and gamma-$Fe_2O_3$ for Selective Catalytic Reduction of Nitrogen Oxides with Ammonia, *Catal. Lett.*, 2013, **143**(7), 697–704.

10 A. Kato, S. Matsuda, T. Kamo, F. Nakajima, H. Kuroda and T. Narita, Reaction between $NO_X$ and $NH_3$ on iron oxide-titanium oxide catalyst, *J. Phys. Chem.*, 1981, **85**(26), 276–287.

11 F. Liu, H. He and C. Zhang, Novel iron titanate catalyst for the selective catalytic reduction of NO with $NH_3$ in the medium temperature range, *Chem. Commun.*, 2008, **164**(17), 2043–2045.

12 F. Liu, H. He, C. Zhang, Z. Feng, L. Zheng, Y. Xie and T. Hu, Selective catalytic reduction of NO with $NH_3$ over iron titanate catalyst: Catalytic performance and characterization, *Appl. Catal., B*, 2010, **96**(3), 408–420.

13 F. Liu, K. Asakura, H. He, Y. Liu, W. Shan, X. Shi and C. Zhang, Influence of calcination temperature on iron titanate catalyst for the selective catalytic reduction of $NO_X$ with $NH_3$, *Catal. Today*, 2011, **164**(1), 520–527.

14 L. Hou, S. Fu, X. Yan, C. Qiao and W. Wu, Effects of sulfate on denitration performance of rare earth tailings for selective catalytic reduction of NO with $NH_3$, *Mol. Cryst. Liq. Cryst.*, 2023, **755**(1), 91–106.

15 P. Zhang, Study on the process mineralogy of large-sized Bayan Obo Fe-REE-Nb deposit, *J. Chin. Rare Earth Soc.*, 1991, **9**(4), 350–353.

16 J. Wang, C. Zhu, B. Li, Z. Gong, Z. Meng, G. Xu and W. Wu, Prepare a catalyst consist of rare earth minerals to denitrate via $NH_3$-SCR, *Green Process. Synth.*, 2019, **9**(1), 191–202.

17 X. Bai, J. Lin, Z. Chen, L. Hou and W. Wu, A Study on the Effect of Different Ball Milling Methods on the $NH_3$-SCR Activity of Aluminum-Laden Bayan Obo Tailings, *Catalysts*, 2021, **11**(5), 568.

18 G. Qi and R. Yang, Low-temperature selective catalytic reduction of NO with $NH_3$ over iron and manganese oxides supported on titania, *Appl. Catal., B*, 2003, **44**(3), 217–225.

19 Z. Chen, F. Wang, H. Li, Q. Yang, L. Wang and X. Li, Low-Temperature Selective Catalytic Reduction of $NO_X$ with $NH_3$ over Fe-Mn Mixed-Oxide Catalysts Containing $Fe_3Mn_{30}$s Phase, *Ind. Eng. Chem. Res.*, 2012, **51**(1), 202–212.

20 B. Shen, T. Liu, N. Zhao, X. Yang and L. Deng, Iron-doped Mn-Ce/$TiO_2$ catalyst for low temperature selective catalytic reduction of NO with $NH_3$, *J. Environ. Sci.*, 2010, **22**(9), 1447–1454.

21 F. Wang, B. Shen, S. Zhu and Z. Wang, Promotion of Fe and Co doped Mn-Ce/$TiO_2$ catalysts for low temperature $NH_3$-SCR with $SO_2$ tolerance, *Fuel*, 2019, **249**, 54–60.

22 E. Hartley and M. J. Matteson, Sulfur dioxide reactions with ammonia in humid air, *Ind. Eng. Chem. Fundam.*, 1975, **14**(1), 67–72.

23 Z. Gao, W. Yang, X. Ding, G. Lv and W. Yang, Support effects in single atom iron catalysts on adsorption characteristics of toxic gases ($NO_2$, $NH_3$, $SO_3$ and $H_2S$), *Appl. Surf. Sci.*, 2018, **436**, 585–595.

24 L. Liu and Z. Yuan, Ordered Mesoporous Carbon Materials Synthesized by Organic-Organic Self-Assembly, *Prog. Chem.*, 2014, **26**(05), 756–771.

25 X. Zhu, Y. Wang, Y. Huang and Y. Cai, Selective catalytic reduction of NO with $NH_3$ over Ce-W-Ti oxide catalysts prepared by solvent combustion method, *Appl. Sci.*, 2018, **8**(12), 2430.

26 F. Liu and H. He, Structure-Activity Relationship of Iron Titanate Catalysts in the Selective Catalytic Reduction of $NO_X$ with $NH_3$, *J. Phys. Chem. C*, 2010, **114**(40), 16929–16936.

27 X. Huang, P. Wang, J. Tao and Z. Xi, $CeO_2$-modified Mn-Fe-O composites and their catalytic performance for $NH_3$-SCR denitrification, *J. Inorg. Mater.*, 2020, **35**(05), 573–580.

28 Q. Fu, J. Wen, L. Li, Y. Xiao and K. Gao, The Study of REE Occurrence State in Bayan Obo Tailings, *Chin. Rare Earths*, 2017, **38**(05), 103–110.

29 J. Sun, Y. Lu, L. Zhang, C. Ge, C. Tang, H. Wan and L. Dong, Comparative Study of Different Doped Metal Cations on the Reduction, Acidity, and Activity of $Fe_9M_1O_X$ (M= $Ti^{4+}$, $Ce^{4+/3+}$, $Al^{3+}$) Catalysts for $NH_3$-SCR Reaction, *Ind. Eng. Chem. Res.*, 2017, **56**(42), 12101–12110.

30 G. Ramis and M. A. Larrubia, An FT-IR study of the adsorption and oxidation of N-containing compounds over $Fe_2O_3/Al_2O_3$ SCR catalysts, *J. Mol. Catal. A: Chem.*, 2004, **215**(1–2), 161–167.

31 A. A. Ioffe, V. P. Bulatov, V. A. Lozovsky, M. Y. Goldenberg, O. M. Sarkisov and S. Ya, Umansky. On the reaction of the $NH_2$ radical with $SO_2$ at 298–363 K, *Chem. Phys. Lett.*, 1989, **156**(5), 425–432.

32 D. Ye, R. Qu, C. Zheng, K. Cen and X. Gao, Mechanistic investigation of enhanced reactivity of $NH_4HSO_4$ and NO on Nb- and Sb- doped V-W/Ti SCR catalysts, *Appl. Catal., A*, 2018, **549**, 310–319.

33 F. Liu and H. He, Selective catalytic reduction of NO with $NH_3$ over manganese substituted iron titanate catalyst: Reaction mechanism and $H_2O/SO_2$ inhibition mechanism study, *Catal. Today*, 2010, **153**(3–4), 70–76.

34 L. Chen, X. Yao, J. Cao, F. Yang, C. Tang and L. Dong, Effect of $Ti^{4+}$ and $Sn^{4+}$ co-incorporation on the catalytic performance of $CeO_2$-$MnO_X$ catalyst for low temperature $NH_3$-SCR, *Appl. Surf. Sci.*, 2019, **476**, 283–292.

35 F. Gao, X. Tang, H. Yi, S. Zhao, J. Wang and T. Gu, Improvement of activity, selectivity and $H_2O\&SO_2$-tolerance of micro-mesoporous $CrMn_2O_4$ spinel catalyst for low-temperature $NH_3$-SCR of $NO_X$, *Appl. Surf. Sci.*, 2019, **466**, 411–424.

36 S. Pan, H. Luo, L. Li, Z. Wei and B. Huang, $H_2O$ and $SO_2$ deactivation mechanism of $MnO_X$/MWCNTs for low-temperature SCR of $NO_X$ with $NH_3$, *J. Mol. Catal. A: Chem.*, 2013, **377**, 154–161.

37 T. Gu, L. Yue, H. Wang and Z. Wu, The enhanced performance of ceria with surface sulfation for selective catalytic reduction of NO by $NH_3$, *Catal. Commun.*, 2010, **12**(4), 310–313.

38 W. S. A. El-Yazeed, M. Eladl, A. I. Ahmed and A. A. Ibrahim, Sulfamic: acid incorporated tin oxide: Acidity and activity relationship, *J. Alloys Compd.*, 2021, **858**, 158–192.

39 E. Hayon, A. Treinin and J. Wilf, Electronic spectra, photochemistry, and autoxidation mechanism of the sulfite bisulfite pyrosulfite systems. SO2-, SO3-, SO4-, and SO5-radicals, *J. Am. Chem. Soc.*, 1972, **94**(1), 47–57.